Early freezing dynamics of an aqueous foam

Krishan Bumma, Axel Huerre, Juliette Pierre, Thomas Séon

Early freezing dynamics of an aqueous foam

Krishan Bumma, Axel Huerre, Juliette Pierre, Thomas Séon

Early freezing dynamics of an aqueous foam†

Krishan Bumma,*[a] Axel Huerre,[b] Juliette Pierre,[a] and Thomas Séon[a]

Liquid foam freezing is an essential and unavoidable processing to obtain solid foam. We study experimentally the solidification dynamics of a model aqueous foam in contact with a cold substrate. The substrate temperature, the foam bubble radius and the liquid fraction are changed. We show that the freezing dynamics always starts by following a self similar square root of time diffusive dynamics. This early dynamics is then predicted as a function of the control parameters using a 1D diffusion model and by treating our foam as a homogeneous fluid with equivalent thermophysical properties. In particular, we build a new expression for the foam conductivity. Finally, experimental and theoretical results are compared and interpreted. This study paves the way towards the understanding of the complex foam freezing dynamics at longer time, when the freezing is then coupled to water migration in the foam.

The freezing of a porous material initially filled with a liquid is a widely encountered phenomenon. Among its many natural occurrences we can cite the upward displacement of ground surface, called frost heave, caused by the formation of ice lenses within the underlying soil[1–3]; and the frost hardiness of terrestrial plants due to ice formation in specific intercellular and extracellular spaces that induces freezing avoidance within dehydrated living cells[4–6]. From an industrial standpoint, understanding and controlling the freezing of porous materials is essential for cryosurgery and cryo-preserving food, plants, and animals[7]. The quality of frozen products depends on the size of the ice crystals, the degree of cell dehydration, and the amount of damage to the cell walls. All of these factors are determined by the rate of freezing[8].

A solid foam consists of pockets of gas surrounded by solid walls. For example, the sea sponge is an open-cell foam that allows water to penetrate and retains it by capillary action. Since the foam properties are so interesting, many artificial foams have been created, such as polymeric and metallic foams[9]. Most polymeric foams are created by the formation of gas bubbles in a melt or liquid system through nucleation, growth, and expansion. These foams then solidify through a complex physico-chemical process influenced by many variables controlling the final product. It is typically achieved through thermosetting of molten thermoplastic polymers that harden as the foam expands or cools down[10]. In contrast, solid metal foam is produced through a different process. A melt is foamed using a blowing agent that releases gas, and the resulting liquid foam is cooled at the precise moment before the liquid foam collapses[11]. This process freezes the unstable foam structure in a solid state, resulting in solid metal foam[11]. These particular foams are widely used due to their impressive properties: softness, light weight, yet strength, as well as useful thermal and acoustic insulation, and energy absorption capabilities. In each of these process, the freezing of liquid foam is an essential and unavoidable processing to obtain solid foam. However, foam solidification have been the object of only very few studies[12,13].

In this paper, we propose to investigate the freezing of an aqueous foam. We begin by describing the experimental setup and then analyze the freezing dynamics of the foam by changing the temperature and bubble radius, as well as the liquid fraction. To predict the freezing dynamics, we treat the foam as a homogeneous fluid with equivalent thermophysical properties and propose a new expression for the foam conductivity. Finally, we compare and interpret the experimental and theoretical results.

1 Experimental setup

The experiment consists in freezing a liquid aqueous foam contained in a tube and placed on a cold substrate, as shown in the schematic of Figure 1(a). The foams are made by mixing a 10 g/L sodium dodecyl sulfate (SDS) solution and perfluorohexane (C_6F_{14}) saturated air, using a cyclic diphasic flow through the constriction made by two linked syringes[14]. Fluorescent dye is added to help the visualisation. The liquid fraction ϕ_l, defined as the volume percentage of liquid in the foam, is selected *a priori* by introducing the right amount of soapy solution and gas in the syringes and precisely measured *a posteriori* by weighing a controlled volume of foam. ϕ_l ranges from 3% to 27% in our experiments. Foams dryer than 3% are not achievable by this method. The liquid fraction is considered unaffected by gravity as the Bond number, $\mathrm{Bo} = \rho g R H/\gamma$ with ρ the liquid density, g the gravity, γ the surface tension, R the characteristic bubble radius, and H the foam height, that compares the capillary pressure at the bubble scale and the hydrostatic pressure on the foam height, is smaller than 1 (around 0.1)[9].

The bubble size distribution is measured *a posteriori*, by dispersing the foam at the surface of the soapy solution to obtain a monolayer of bubbles and then measuring their diameters using a microscope[15]. With our 20 mL syringes the bubble size distribution is reproducible and the average bubble size is around $R = 25\ \mu$m. The typical bubble size distribution is show in the supplementary material†. By using C_6F_{14} saturated air, we ensured that the foams do not undergo coarsening during the time of our experiments. Indeed, the typical time needed to double the average bubble size of such a foam is of a few hours, while the freezing experiment is at most 15 minutes long. The average bubble size measured initially is then not affected by coarsening during the freezing process. However, it can be increased signifi-

[a] *Institut Jean Le Rond ∂'Alembert, CNRS UMR 7190,Sorbonne Université, Paris, France; E-mail : krishan.bumma@dalembert.upmc.fr*

[b] *Laboratoire Matière et Systèmes Complexes, CNRS UMR 7057, Université Paris Cité, Paris, France*

† Electronic Supplementary Information (ESI) available: [detailled detailled resolution of the heat equation,]. See DOI:

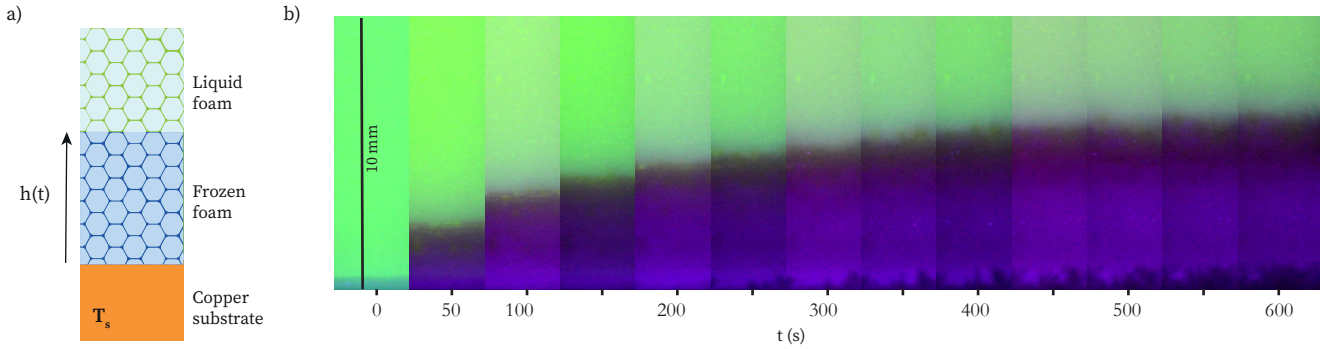

Fig. 1 a) Schematic of the experiment b) Time sequence of a foam freezing experiment with liquid fraction $\phi_l = 13\%$ and substrate temperature $T_s = -30.2°C$. The liquid foam appears green due to the fluorescein only fluorescing in the liquid phase. The frozen layer, appearing purple under UV light, undergoes fast growth in the first seconds before slowing down.

cantly by waiting at least 3 hours before freezing the foam. This way, a few experiments are done with average bubble size foam of $R = 48$ μm and 86 μm.

Once produced and characterised, the foam is poured into a cylindrical plastic tube with inner diameter 1.2 cm and height 4.8 cm. We observe that the foam sticks to the walls of the tube. The tube wall is thin enough, down to 100 μm, to limit the vertical heat flux through it. Moreover, the very low thermal conductivity of the air allows us to safely neglect the heat flux in the air and to consider the plastic tube as insulating. The tube filled with the foam is then placed vertically on a copper surface (see Fig. 1 (a)) cooled down using a refrigerated circulator (Julabo CORIO CD-1000F). This enables the substrate to maintain a constant temperature in the range -14°C $\leq T_s \leq$-32°C during the 15 minutes experiments. Temperatures down to $-105°$C were also achieved using liquid nitrogen to cool the substrate.

Finally, the freezing foam is observed under ultra-violet (UV) light with a 200 mm macro lens mounted on a Nikon D800 with a 52.5 mm long-extension tube. Typically obtained images are presented in the time sequence of Figure 1 (b), where the liquid foam appears bright green because of the fluorescent dye, and the solid foam appears dark as the fluorescent molecules are largely expelled from the growing ice [16].

2 Experimental Results

In this time sequence (Fig. 1 (b)), a slab of foam of 10 mm right above the cold substrate ($T_s = -30.2°$C) is displayed as a function of time. At t=0 the foam is entirely liquid, but very rapidly the foam solidifies and we observe the dark solid foam growing and decelerating with time. The height of the freezing front, $h(t)$, is then measured and plotted with black dots as a function of time in the inset of Figure 2(a). The qualitative observation is confirmed, the freezing starts quickly and then slows down with time. The main plot of Figure 2(a) presents the same experimental data in logarithmic scale. Two regimes are observed : a first regime where the data aligns along a dashed line of slope 1/2 meaning that the height of the frozen foam grows following the square root of time, and then enters a slower second regime after a few hundred seconds. The dashed line of slope 1/2 fitting the experimental diffusive regime can be expressed as $h(t) = \sqrt{D_{\text{eff}}^{\text{exp}} t}$, where $D_{\text{eff}}^{\text{exp}}$ is an effective diffusive coefficient determined experimentally. The existence of these two regimes of front propagation, starting with a diffusive regime, is typical of systems where diffusion and convection play a role with different time scales [17,18]. In these experiments, convection in the liquid foam might lead to a water supply at the freezing front, impacting the diffusive growth after a certain time. However, the mechanisms leading to water convection are not clear at all. The appearance of this second regime is then beyond the scope of this study focused on the quantitative description of the first diffusive regime of freezing foam. Therefore, the following panels on Figure 2 present only the results for this early-time regime.

In Figure 2(b), the solidification dynamics in the first regime for a foam, with the same liquid fraction $\phi_l \sim 16.5\%$ and mean bubble size $R = 25\mu$m, is plotted for three different substrate temperature: $T_s = -39.9°$C, $-69.8°$C and $-96.0°$C. We notice that the three curves have the same shape on a log-log scale with a freezing dynamics following a square root of time. The curves are ordered by temperature, with colder substrates causing faster solidification of a given volume of foam: the effective diffusive coefficient depends on the temperature and, as expected, is larger for colder substrates. Figure 2(c) presents the solidification dynamics in logarithmic scale for foams with three liquid fractions $\phi_l = 12.7$, 18.8, and 26.9% but same mean bubble size $R = 25\,\mu$m and same substrate temperature $T_s = -20°$C. The experiments always follow the square-root dynamics but are shifted: the effective diffusive coefficient clearly depends on the liquid fraction. From these curves it seems that the wetter the foam (high liquid fractions, darker symbols) the faster the freezing dynamics. Finally, Figure 2(d) shows foams freezing with different bubble size distributions†, with mean bubble sizes: $R = 23$, 48 and 86 μm, all other parameters being equal: $\phi_l \sim 10\%$ and $T_s = -30°C$. At early times, we recover the square root of time regime and all the curves are superimposed. Therefore, it seems that the bubble radius does not influence the solidification dynamics during the first regime.

In the following sections of the paper, we focus on building a physical model that predicts the effective diffusion coefficient

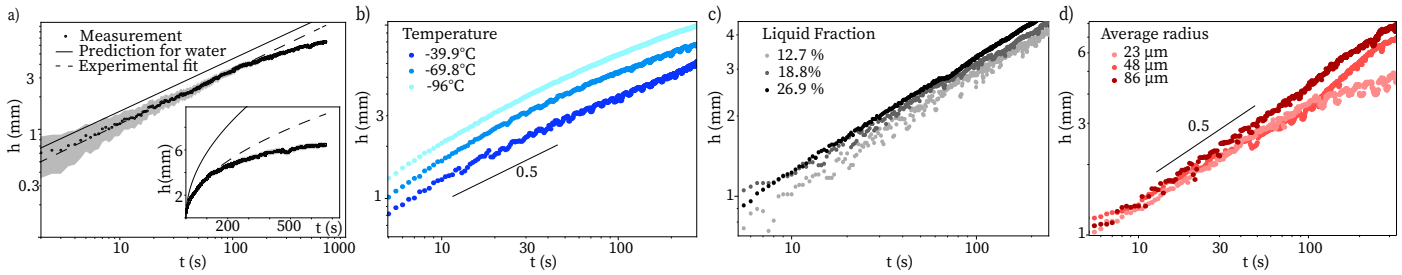

Fig. 2 (a) Height of the freezing front for $T_s = -30.2°C$, $R = 25\mu m$, and $\phi_l = 13\%$. The grey zone represents the uncertainty of the automated measurements, estimated at 15 pixels on the original images, it is about 0.2 mm. The solid line is the result of the 1D model for pure water, and the dashed line is a 1/2 power-law fit of the experimental data. (b) $h(t)$ measured for $\phi_l \sim 16.5\%$ and $R = 25\mu m$ for temperatures $T_s = -39.9°C$, $-69.8°C$ and $-96.0°C$. The solid line is the $1/2$ slope. (c) $h(t)$ measured for $T_s = -20 \pm 1°C$ and R$= 25\mu m$ for $\phi_l = 12.7\%$, 18.9% and 26.9%. (d) $h(t)$ measured for $T_s = -30 \pm 1°C$ and $\phi_l = 10 \pm 1\%$ for 3 different radii R$= 23\mu m$, $48\mu m$, and $86\mu m$.

$D_{\text{eff}}^{\text{th}}$ of a one dimensional foam freezing and compare it with our experimental measurements. As observed experimentally in Figure 2, the diffusion coefficient has to vary with the substrate temperature T_s and the liquid fraction in the foam ϕ_l but not with the average bubble size R.

3 Predicting the freezing dynamics

3.1 Stefan model

The freezing front propagation dynamics for a one-dimensional liquid system is known as the Stefan problem[19]. The growth of the solid layer follows the classical diffusive dynamics: $h(t) = \sqrt{D_{\text{eff}} t}$, where D_{eff} is an effective diffusion coefficient that depends on the temperatures at the boundaries and the thermal properties of the two phases[20]. When a layer of ice rests between a semi-infinite solid substrate and semi-infinite water, a variant of the Stefan problem exists[21–23]. To find it one consider the 1-D heat equations in the substrate, in the ice and in the water, one write the continuity of temperature and heat fluxes at the ice-substrate interface, and the discontinuity of heat fluxes due to latent heat at the ice-water interface. This way one obtain an implicit relationship between D_{eff}, the substrate temperature T_s, and the thermal parameters of the water, the ice, and the substrate. This equation can be solved numerically to obtain D_{eff}. It was computed for the experimental configuration of Figure 1 and the resulting dynamics for the ice front propagation is plotted as a solid line in Figure 2(a). This prediction of freezing dynamics for water lies above the fit of the experimental freezing dynamics for foam in the diffusive regime (dashed line): the freezing front propagates much faster in water than in our foam. Experimental freezing of the soapy water shows no difference with freezing of distilled water, so the difference observed between the freezing of a foam and of water lies in the physical characteristics of the foam. Figure 2(b) confirms this difference as $D_{\text{eff}}^{\text{exp}}$ appears to be dependent on the foam liquid fraction ϕ_l. Therefore, to predict the freezing dynamics of a foam, the geometrical configuration (randomly oriented Plateau borders, vertices, soap films) and the physical properties of the phases (liquid and encapsulated gas) have to be taken into account.

3.2 Foam conductivity

We will consider the foam as a homogeneous fluid with effective thermo-physical properties and in particular, an effective thermal conductivity. This treatment is classical and has been used in many other examples of heat conduction through heterogeneous media[24,25]. The problem of heat conduction in heterogeneous materials is mathematically analogous to the problem of electrical conductivity in such materials[26]. Maxwell was the first to give analytical expressions for the effective conductivity of an heterogeneous medium in his famous work on electricity and magnetism[27]. He considered the problem of dilute dispersion of spherical inclusions, namely the *very-wet* limit. In the case of air bubbles in water the expression for the effective conductivity reduces to $2\phi_l\lambda_l/(3-\phi_l)$, with λ_l the conductivity of water. Naturally, the other limit is a *very-dry* foam, where bubbles are tightly compressed in a small volume of liquid and form a network of randomly oriented Plateau borders at which three soap films meet. In this limit, the effective conductivity of the foam is given by Lemlich's expression[28]: $\phi_l\lambda_l/3$.

The foams considered here have intermediate liquid fractions and thus their conductivities lie between these two limits. We propose to build an expression that accounts for the foam structure evolution between the *very-dry* and *very-wet limits*. In a very-dry foam, $\phi_l \to 0$, the water is mainly along the length of the Plateau borders and not in the vertices (where Plateau borders meet in fours), forming mostly 1D structures. Then when ϕ_l increases to reach the very-wet limit, $\phi_l \to \phi_{lc} = 0.33$, the foam becomes a suspension of spheres and Plateau borders no longer exist, the water is in what would be the vertices: 3D liquid structures between 4 bubbles. Note that the films are considered to contain a negligible amount of water, not contributing significantly to the conductivity. In the aim of expressing the conductivity of the liquid matrix of the foam, we propose to weigh the Lemlich's expression by the proportion of liquid in Plateau borders and to add Maxwell's expression weighed by its complement, the proportion of vertices. Lacking an exact expression for the proportion of Plateau borders relative to vertices, we will take $1 - \phi_l/\phi_{lc}$ as the proportion of Plateau borders. This function of ϕ_l goes to 1 when the foam is dry and the liquid is within the straight segments of the Plateau borders, and goes to 0 at $\phi_l = \phi_{lc}$, when the bubbles are at close

packing and surrounded only by vertices. The proposed expression of the conductivity of the liquid matrix is thus:

$$\lambda_{\text{matrix}} = \frac{1}{3}\phi_l\lambda_l\,(1-\phi_l/\phi_{lc}) + \frac{2}{3-\phi_l}\phi_l\lambda_l\phi_l/\phi_{lc} \qquad (1)$$

This new theoretical expression of the conductivity of the foam can be compared to experimental data on electric conductivities. Figure 3(a) shows measurements of the electrical conductivity of foams for liquid fractions between 1 and 30%. These data are realised or extracted from the literature by Feitosa *et al.*[9,29]. The dashed line represents a one-parameter best-fit to the data, proposed by the authors, that describes all the data well and, in particular, works better than the previous ones[10,30] for the intermediate liquid fractions. This convenient fit is a rational function formed by the ratio of second-order polynomials. The model proposed here (Eq. (1)) is plotted as a black solid line and shows an excellent agreement with the experimental values. Therefore this new model works well, has no adjustable parameter and is built using physical arguments.

The net heat transfer in a foam is the superposition of the conduction and the radiation considered separately[31]. The thermal conductivity of a foam can thus be expressed as the sum of these different contributions: the conduction through the foam matrix (solid or liquid) which is analogous to the electrical conduction and therefore given by the Eq. (1), and the two contributions that take place inside the bubbles, namely the conduction through air and the radiation. For the thermal conductivity of the gas phase, we will simply weight the conductivity of air λ_{air} by the amount of air, $1-\phi_l$, neglecting the contribution of the films. As we use relatively wet foams ($>5\%$) with small bubbles ($\sim 100\,\mu m$), radiation can be neglected[25,31].

Finally, we end up with the following expression for the thermal conductivity of foam :

$$\lambda^{l,s}_{\text{foam}} = (1-\phi_l)\lambda_{air} + \frac{1}{3}\phi_l\lambda_{l,s}\,(1-\phi_l/\phi_{lc}) + \frac{2}{3-\phi_l}\phi_l\lambda_{l,s}\phi_l/\phi_{lc} \qquad (2)$$

The superscripts l and s stand for liquid and solid, here water and ice. In this expression, we observe that neither the average bubble size distribution, nor the interfacial properties play a role.

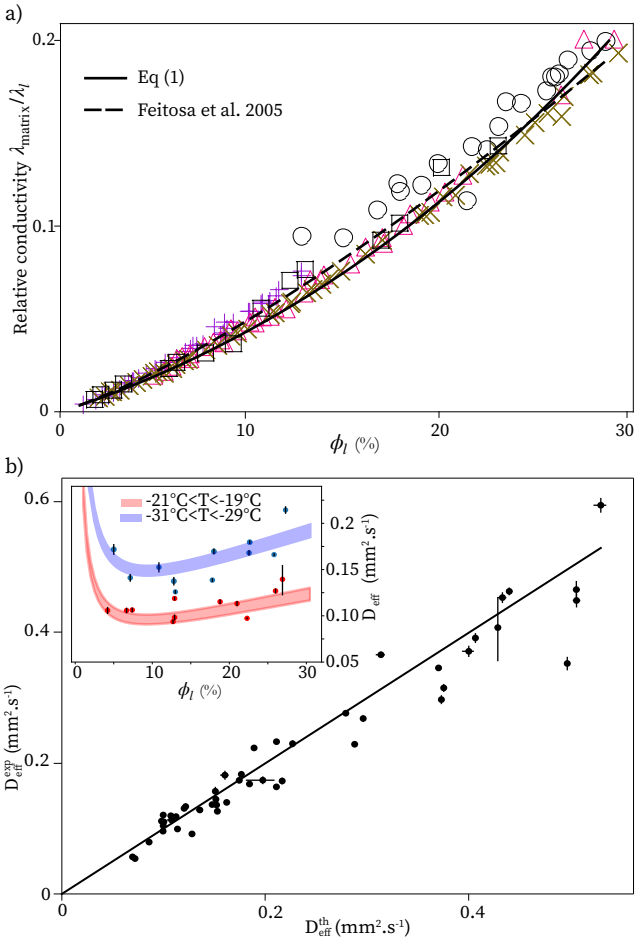

Fig. 3 (a)Electrical conductivity of the foam relative to the conductivity of the liquid, as a function of the liquid fraction (experimental data from[29]). The dashed line is a fit of the data proposed in[29]. The solid line shows our prediction based on Eq. (1). (b) Experimental measurement of D_{eff}, plotted against the predicted value of D_{eff} for experiments with radii between 18μm and 30μm for temperatures ranging from $-14°$C to $-105°$C. The measurement of this effective diffusion coefficient is obtained by fitting a square root to the first 100 s of our experimental measurement $h(t)$. Inset: Experimental measurement of D_{eff} for experiments done at -20 and -30°C for varying liquid fractions. The blue and red regions represent the predicted value of D_{eff} at $-20\pm1°$C and $-30\pm1°$C.

3.3 Related Stefan problem

The Stefan problem can now be solved as described previously, considering the foam as an effective medium, with conductivity $\lambda^{l,s}_{\text{foam}}$ defined by Equation (2). We assume in the following that the foam solidifies keeping the same porosity $1-\phi_l$, and only the conductivities of the water is changed to the one of ice after foam freezes.

The Stefan condition describing phase change in our case is then written as:

$$\phi_l\rho_s\mathscr{L}\frac{\mathrm{d}h}{\mathrm{d}t} = \lambda^s_{\text{foam}}\frac{\partial T}{\partial z}(h^-) - \lambda^l_{\text{foam}}\frac{\partial T}{\partial z}(h^+) \qquad (3)$$

with $\mathscr{L}$ the latent heat of solidification of the water solution, and ρ_s the density of ice. The resolution of this Stefan problem for given values of liquid foam and substrate temperatures gives the prediction of the freezing front propagation dynamics in the foam

$h(t) = \sqrt{D_{\text{eff}}^{\text{th}} t}$ (see Supplementary Materials for details [†]).

The experimental value of $D_{\text{eff}}^{\text{exp}}$ is plotted as a function of the theoretical prediction $D_{\text{eff}}^{\text{th}}$ in Figure 3(b) for substrate temperatures ranging from -14°C to -105°C, liquid fractions between 3 and 27% and mean bubble radii between 18 and 30 μm. The solid line represents $D_{\text{eff}}^{\text{exp}} = D_{\text{eff}}^{\text{th}}$. This plot shows the good agreement between our model and the solidification behaviour of the foam during the first hundred seconds of the experiment that defines the diffusion regime of foam solidification.

The inset of Figure 3(b) presents the variation of the effective diffusion coefficient with liquid fraction. Two series of experiments at $T_s = -20 \pm 1^\circ$ and $-30 \pm 1^\circ$C are plotted for liquid fractions varying between 3 and 28%. The experimental measurements are plotted with dots and theoretical prediction with two thick lines corresponding to the two substrate temperatures. As the experiments are realized at temperatures that can be slightly different in the given range, the prediction is given in the same range represented by the thickness of the two lines. As expected, the comparison between experimental measurements and theoretical prediction is satisfying. For liquid fraction higher than $\phi_l \sim 7-8\%$, the wetter the foam, the faster it freezes. This is what was observed in Figure 2(c), or in Figure 2(a) where the freezing is observed faster in a liquid column than in a foam, and is explained by a better conduction of heat in ice than in water.

However, counter-intuitively we predict that the curve is non-monotonic and dry foams ($\phi_l < 5\%$) freeze faster than wetter ones. Indeed, the thermal conductivity of the foam does not tend to zero when the liquid fraction tends to zero. Consequently, the heat exchanged through the gas phase is small but significant compared to the very small amount of water to freeze. This non-monotonic variation of the effective diffusion coefficient with liquid fraction is predicted theoretically and confirmed experimentally.

4 Conclusion and perspective

In this study, it is shown that the freezing of an aqueous foam starts by following a self-similar square root of time-diffusive dynamics. A new model for the foam conductivity, physical, taking into account the foam structure, and without adjustable parameters is proposed. A good agreement is found between experimental measurements and theoretical prediction for the front propagation dynamics, highlighting the key role of the liquid fraction in the freezing dynamics. In the experiment, we show that after about a hundred seconds the freezing foam leaves its diffusive regime and the freezing slows down. In the model, it is assumed that the foam porosity $(1-\phi_l)$ stays constant when it freezes. Most probably, the freezing dynamics loses its diffusive character when this strong assumption is broken and the porosity starts to change while the foam freezes. The understanding of mechanisms at the origin of this modification of the foam structure when it solidifies and the characterisation and prediction of the evolution of the foam porosity constitute interesting leads for future research.

Conflicts of interest

There are no conflicts to declare.

Notes and references

1 S. Taber, *The Journal of Geology*, 1930, **38**, 303–317.
2 A. Rempel, *Journal of Geophysical Research: Earth Surface*, 2007, **112**, year.
3 S. S. Peppin and R. W. Style, *Vadose Zone Journal*, 2013, **12**, year.
4 A. Sakai and W. Larcher, *Frost survival of plants: responses and adaptation to freezing stress*, Springer Berlin Heidelberg, 1987, vol. 62.
5 E. H. Beck, S. Fettig, C. Knake, K. Hartig and T. Bhattarai, *Journal of biosciences*, 2007, **32**, 501–510.
6 L. V. Gusta and M. Wisniewski, *Physiologia plantarum*, 2013, **147**, 4–14.
7 C. Körber, *Quarterly reviews of biophysics*, 1988, **21**, 229–298.
8 M. S. Rahman, *Handbook of food preservation*, CRC press, 2007.
9 I. Cantat, S. Cohen-Addad, F. Elias, F. Graner, R. Höhler, O. Pitois, F. Rouyer and A. Saint-Jalmes, *Foams: structure and dynamics*, OUP Oxford, 2013.
10 D. L. Weaire and S. Hutzler, *The physics of foams*, Oxford University Press, 2001.
11 J. Banhart and D. Weaire, *Physics Today*, 2002, **55**, 37–42.
12 S. Cox, G. Bradley and D. Weaire, *The European Physical Journal-Applied Physics*, 2001, **14**, 87–96.
13 M. Mukherjee, F. Garcia-Moreno and J. Banhart, *Acta Materialia*, 2010, **58**, 6358–6370.
14 T. Gaillard, M. Roché, C. Honorez, M. Jumeau, A. Balan, C. Jedrzejczyk and W. Drenckhan, *International Journal of Multiphase Flow*, 2017, **96**, 173–187.
15 J. Pierre, R.-M. Guillermic, F. Elias, W. Drenckhan and V. Leroy, *The European Physical Journal E*, 2013, **36**, 1–10.
16 M. Marcellini, C. Noirjean, D. Dedovets, J. Maria and S. Deville, *ACS omega*, 2016, **1**, 1019–1026.
17 A. Monier, A. Huerre, C. Josserand and T. Séon, *Physical Review Fluids*, 2020, **5**, 062301.
18 A. Huerre, A. Monier, T. Séon and C. Josserand, *Journal of Fluid Mechanics*, 2021, **914**, year.
19 L. Rubinstein, *The Stefan Problem*, American Mathematical Soc., 1971, vol. 27.
20 G. Lamé and B. Clapeyron, Annales Chimie Physique, 1831, pp. 250–256.
21 H. S. Carslaw and J. C. Jaeger, *Oxford: Clarendon Press, 1959, 2nd ed.*, 1959.
22 V. Thiévenaz, T. Séon and C. Josserand, *J. Fluid Mech.*, 2019, **874**, 756–773.
23 P. Kant, R. B. Koldeweij, K. Harth, M. A. van Limbeek and D. Lohse, *Proceedings of the National Academy of Sciences*, 2020.
24 K. Boomsma and D. Poulikakos, *International Journal of Heat and Mass Transfer*, 2001, **44**, 827–836.
25 M. Kaviany, *Principles of heat transfer in porous media*, Springer Science & Business Media, 2012.

26 K. Pietrak and T. S. Wiśniewski, *Journal of Power Technologies*, 2015, **95**, year.

27 J. C. Maxwell, *A treatise on electricity and magnetism*, Clarendon press, 1873, vol. 1.

28 R. Lemlich, *Journal of colloid and Interface Science*, 1978, **64**, 107–110.

29 K. Feitosa, S. Marze, A. Saint-Jalmes and D. Durian, *Journal of Physics: Condensed Matter*, 2005, **17**, 6301.

30 R. Lemlich, *Industrial & Engineering Chemistry Process Design and Development*, 1985, **24**, 686–687.

31 N. Hilyard and A. Cunningham, *Low density cellular plastics: Physical basis of behaviour*, Springer Science & Business Media, 2012.